Received: 3 August 2016 | Accepted: 20 October 2016

DOI: 10.1002/pro6.6

ORIGINAL ARTICLE

WILEY

Finding of dose evaluation for organs at risk in intensity-modulated radiation therapy for nasopharyngeal carcinoma using magnetic resonance imaging

Guanzhong Gong[1,2] | **Xudong Kong**[3] | **Xiuying Wang**[1] | **Chaojie Zheng**[1] | **Yujie Guo**[2] | **Yong Yin**[2]

[1]Biomedical and Multimedia Information Technology (BMIT) research group, School of Information Technologies (SIT), The University of Sydney, New South Wales, Australia

[2]Shandong Cancer Hospital and Institute, Jinan Shandong, China

[3]The No. 4 Hospital of Wuxi, Wuxi Jiang Su province, China

Correspondence
Xiuying Wang, Biomedical and Multimedia Information Technology (BMIT) Research Group, School of Information Technologies (SIT), The University of Sydney, NSW 2008, Australia.
Phone: +61-0417204265;
Fax: +61-935133788.
Email: xiu.wang@sydney.edu.au
Yong Yin, Shandong Cancer Hospital and Institute, Jiyan Road 440#, Jinan Shandong 250117, China.
Phone: +86-531-6762-6427;
Fax: +86-531-67626427.
Email: yinyongsd@126.com

Funding Information
National Natural Science Fund of China, Grant/Award Number: 81301936, 81472811, and 81530060

Abstract

A critical step in predicting and avoiding radiation injury of organs at risk in radiation therapy of nasopharyngeal carcinoma is to carry out an accurate dose evaluation in planning design. In the present study, we investigated the dose evaluation feature of organs at risk on magnetic resonance imaging (MRI) images in intensity-modulated radiation therapy of nasopharyngeal carcinoma compared with computed tomography (CT) images. A total of 35 nasopharyngeal carcinoma patients were selected for this trial. CT simulation with non-contrast and contrast-enhanced scan, and MRI simulation with non-contrast and contrast-enhanced T1, T2, and diffusion weighted imaging were obtained sequentially. The organs at risk were contoured on the CT and MRI images after rigid registration, respectively. Nine-beam intensity-modulated radiation therapy plans with equal division angles were designed for every patient, and the prescription dose for the tumor target was set as 72 Gy (2.4Gy/fraction). The boundary display, volume, and dosimetric indices of each organ were compared between MRI and CT images. We found that MRI showed clearer boundary of the brainstem, spinal cord, deep lobe of the parotid gland, and the optical nerve in the canal compared with CT. MRI images increased the volume of the lens and optic nerve, while slightly reducing the volume of eye; the maximum dose of the lens, and the mean dose of the eyes and optic nerve increased to different extents, though no statistical differences were found. The left and right parotid gland volume on MRI increased by 7.07% and 8.13%, and the mean dose increased by 14.95% (4.01 Gy) and 18.76% (4.95 Gy), with a statistically significant difference ($P < 0.05$). The brainstem volume reduced by 9.33% ($P < 0.05$), and the dose of 0.1 cm^3 volume reduced by a mean 8.46% (4.32 Gy), whereas the dose of 0.1 cm^3 of the spinal cord increased by 1.5 Gy on MRI. The maximum dose region of the spinal cord was very close on CT and MRI images, and was similar to the brainstem. In conclusion, it is credible to evaluate the radiation dose of the lens, eye, brainstem, and the spinal cord by applying simulation CT; whereas MRI images are sometimes necessary to evaluate the dose of the parotid glands and the optical nerve.

KEYWORDS

computed tomography, dosimetry, intensity-modulated radiation therapy, magnetic resonance imaging, nasopharyngeal carcinoma

1 | INTRODUCTION

Nasopharyngeal carcinoma (NPC) is one of the most common malignant tumors in the world, with the highest incidence occurring in China.[1] NPC patients should receive comprehensive treatment, the mainstay of which is radiotherapy (RT).[2,3] RT has played an irreplaceable role in NPC therapy. However, local recurrence and radiation injury of organs at risk (OAR) are the major factors affecting the survival time and quality of life of NPC patients treated with RT.[4,5] The use of accurate target volume definition approaches and new RT technology has played an important role in improving the rate of local control and the protection of normal OAR. It is well known that magnetic resonance imaging (MRI) plays an important role in the diagnosis, staging, and treatment of NPC, with better soft tissue resolution.[2] In addition, MRI-guided NPC precision radiotherapy has shown good prospects.[5–7]

In the past, the research on MRI-guided NPC radiotherapy mainly focused on accurate target identification and delineation, the identification of metastatic lymph nodes, and the therapeutic effect of radiotherapy during the follow up.[8,9] Recently, the study of OAR contours on MRI images from patients with NPC has become attractive, and Ma Jun's group has published a detailed report about this aspect.[10,11] Previous studies from our research group showed that the parotid gland and brainstem, which are contoured on MRI images for NPC, showed high accuracy and repeatability.[12,13]

Computed tomography (CT) simulation images have been used in tumor position, RT plan design, prediction of clinical outcome, and radiation risk of OAR for decades. With the increase of MRI images in RT of NPC, more studies to investigate the priority of MRI application are underway. In order to verify the dosimetric features that are obtained by the evaluation of the dose–volume indices based on MRI images, we carried out research on the feasibility and difference of radiation dose assessment of OAR that were defined on MRI images, compared with CT simulation images.

2 | METHODS

2.1 | Patient information

The CT and MRI image data of 35 NPC patients who received radiation oncology treatments from 12 October 2012 to 1 January 2015 were analyzed retrospectively. The analysis included 21 male and 14 female (aged 18–55 years) patients, 26 and nine of which were T3 stage and T4 stage, respectively. The study was approved by the No. 4 Hospital of Wuxi Ethics Committee and Shandong Cancer Hospital and Institute.

2.2 | CT and MRI simulation

CT simulation was carried out on the Philips Big Bore CT (Phillips Medical Systems, Highland Heights, OH, USA), and scanning was carried out in non-contrast-enhanced and contrast-enhanced modes sequentially. The scan range was from the top of the head to the level of the angulus ludovici; the image thickness and layer spacing were set as 3 mm, and all the scans were carried out in the spiral mode (pitch 0.938, table speed 30 mm/s).

MRI simulation was carried out on the Philips Achieva 3.0T TX (Phillips Medical Systems) followed by a CT scan, T1 weighted images (T1), T2 weighted images (T2), diffusion weighted images (DWI), and T1 contrast-enhanced weighted images ($T1_{-CE}$), and the scan region ranged from the top of arcus superciliaris to the lower edge of vertebra prominence.

The patient was supine in the CT and MRI scanner, and for the CT scanning a thermoplastic fixation mask and a U-shaped head holder were used to fix the patient's head and neck position, with both hands placed on both sides of the body. In order to ensure the patient posture fixing consistency from CT to MRI scan, marks were painted on the surface of both sides of the jawbone, nose apex, and head holder according to the positioning laser light in the CT simulation room. During the MRI scanning, only the U-shaped head holder was used because the diameter of the MRI head scanning coil was too small to fit into a thermoplastic fixation mask and its association plates, but the position of the nose, eyes, and the jawbone was adjusted by marks on the surface and thermoplastic fixation, which had been shaped in the CT simulation in reference to the laser light in MRI scanning to the laser light during the MRI scanning [14,15].

The CT and MRI images were transmitted into the Varian Eclipse 13.5 (1678 S. Pioneer Road Salt Lake City UT 84104, United States) treatment planning system to design and optimize the radiation therapy plans. The workflow is shown as Figure 1.

2.3 | Images registration and target volume definition

Before contouring the target volumes and organs, the MRI images and contrast-enhanced CT images were registered to non-contrast-enhanced CT images using the global rigid registration technology of Eclipse 13.5, and the skeletal structure was defined as the landmark for evaluating the registration outcome.

The target volumes were determined according to the CT and MRI images referring to the book, "*Image-guided IMRT*", and defined the gross tumor volume, including the gross tumor and metastatic lymph nodes; the clinical target volume (CTV), which is obtained from the gross tumor volume with a 5-mm margin; the CTV_{-2} for high-risk nodal regions; and CTV_{-3} for low-risk nodal regions.[16] Additionally, the planning target volume 1 (PTV_{-1}), PTV_{-2}, and PTV_{-3} were obtained from the CTV, CTV_{-2}, and CTV_{-3}, using the appropriate margins.[17]

2.4 | OAR contour

The lens, optic nerve, eyeball, parotid gland, brainstem, and spinal cord were contoured on non-contrast-enhanced CT relative to contrast-enhanced CT. The contour on MRI T1 image were achieved referring to MRI contrast-T1 and T2 images. The vascular tissues that were contained or close to the organs were removed. The contour of each organ was reviewed and decided by two radiation oncologists and one radiologist, and the process was repeated on CT and MRI at different

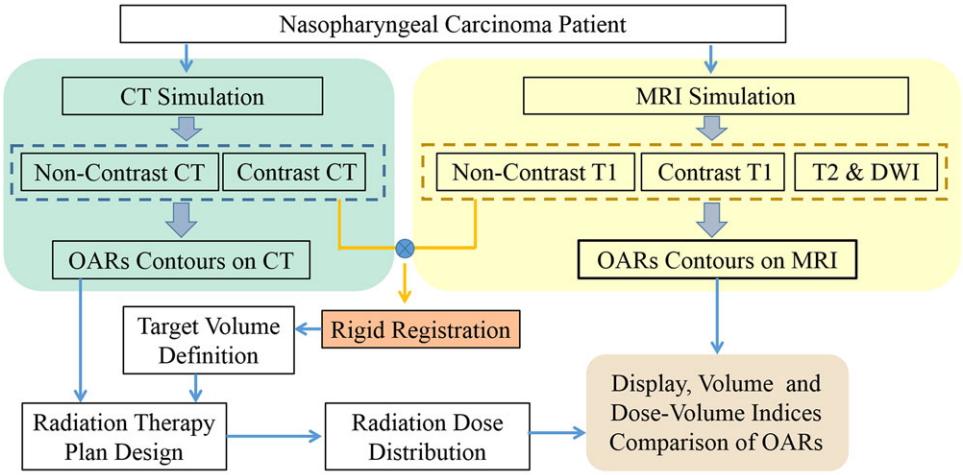

FIGURE 1 The workflow of the present study. CT, computed tomography; MRI, magnetic resonance imaging; OAR, organs at risk

times (intervals of 1–3 days). The upper and lower boundary of each organ on the CT and MRI images were consistent, except for the spinal cord.

2.5 | Treatment plan design and optimization

The intensity-modulated radiation therapy (IMRT) plans with nine equipartition angle fields (0°, 40°, 80°, 120°, 160°, 200°, 240°, 280°, 320°) were designed for NPC patients, and the plans were optimized by a 6-MV X-ray, with a dose calculation grid of 2.5 mm, using the Varian Acuros XB calculation algorithm.[18] All plans were designed and optimized on non-contrast-enhanced CT images, and the limit dose for the organs was calculated and evaluated based on the contours on the CT image. The prescription doses were defined as PTV-1 (72 Gy: 2.4 Gy/fraction × 30 fractions), PTV-N (60 Gy: 2.0 Gy/fraction × 30 fractions) and PTV-p (54 Gy: 1.8 Gy/fraction × 30 fractions).[19]

2.6 | Dose evaluation indices of OAR and data analysis

The maximum dose (D_{-max}) of the lens, the mean dose (D_{-mean}) of the optic nerve, eyeball, and parotid gland, and the dose for the 0.1 cm^3 volume of the brainstem and spinal cord were recorded and compared between the organs contoured on the CT and MRI images.[15,20–22]

The SPSS 16.0 software (IBM, Armonk, NY, USA) was used for the statistical analyses. The paired *t- test* was used to compare the pairwise data. A $P < 0.05$ represents statistical significance.

3 | RESULTS

3.1 | Display differences of the OAR between the MRI and CT

Compared with CT, MRI showed a clearer boundary of the OAR, especially in the optic nerve, brainstem, spinal cord, and deep lobe of the parotid gland, as shown in Figure 2. Additionally, we found that the spinal canal and spinal cord under the second cervical vertebra were displaced with different degrees in 15 cases after registration.

3.2 | Dose–volume differences of the lens, eyeball, and optic nerve between CT and MRI

The lens, eyeball, and optic nerve regions were similar on the CT and MRI images, as shown in Figure 3. Specifically, the optic nerve was extended on the MRI images by 3–5 mm and 5–7 mm in the dorsal direction for 12 patients (left) and 10 patients (right), with a clear boundary of the optic nerve. In addition, the volume of the left

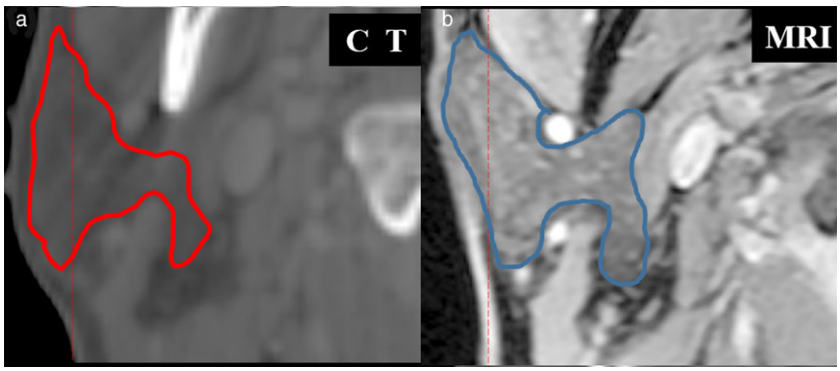

FIGURE 2 The display and contour difference of parotids on (a) computed tomography (CT) and (b) magnetic resonance imaging (MRI) images

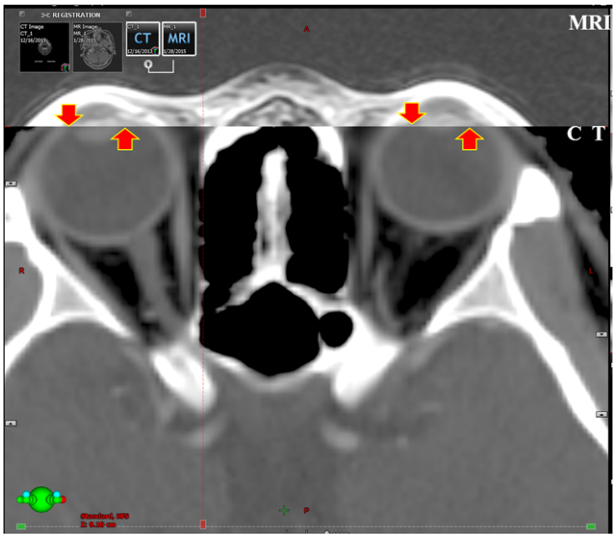

FIGURE 3 The location and region difference of the lens on computed tomography (CT) and magnetic resonance imaging (MRI) images

and right lens increased by a mean of 17.65% (0.3 cm^3) and 11.11% (0.2 cm^3), respectively, but the D_{-max} only increased by a mean of 4.95% (0.18 Gy) and 11.11% (0.41 Gy), without statistically significant differences ($P > 0.05$). Additionally, the D_{-mean} of the eyeball was similar on the CT and MRI images, whereas the D_{-mean} of the left and right optic nerve increased by a mean of 9.69% and 12.15% without statistical significance on MRI images, as shown in Tables 1 and 2.

3.3 | Dose–volume difference of the parotid glands between CT and MRI

The volume of the left and right parotid glands increased by a mean of 7.07% and 8.13%, respectively, on the MRI images; whereas the D_{-mean} increased by a mean of 14.95% and 18.76%, respectively, with all the differences being statistically significant ($P < 0.05$), as shown in Tables 1 and 2.

3.4 | Dose–volume differences of brainstem and spinal cord between CT and MRI

From Tables 1 and 2, it can be seen that the brainstem volume was reduced by a mean of 9.33% on the MRI images, which was statistically significant ($P < 0.05$), as was the mean of 8.46% (4.6 Gy) reduction of the $D_{0.1cm^3}$ ($P > 0.05$). The $D_{0.1cm^3}$ of the spinal cord increased by 1.5 Gy, and the maximum dose region position was nearby in the CT and MRI images.

TABLE 1 Volume differences of organs at risk between computed tomography and magnetic resonance imaging

Organ	CT (cm^3)	MRI (cm^3)	Variation (cm^3)	%	*t*	*P*
$Lens_{-R}$	0.18 ± 0.04	0.20 ± 0.06	0.02	11.11%	1.46	0.16
$Lens_{-L}$	0.17 ± 0.03	0.20 ± 0.08	0.03	17.65%	1.93	0.07
$Optic\ nerve_{-R}$	0.39 ± 0.15	0.46 ± 0.19	0.07	17.95%	1.59	0.13
$Optic\ nerve_{-L}$	0.37 ± 0.12	0.37 ± 0.13	0	0.00%	0.05	0.96
$Eyeball_{-R}$	7.86 ± 0.91	7.76 ± 1.23	−0.1	−1.27%	−0.774	0.448
$Eyeball_{-L}$	7.82 ± 1.07	7.69 ± 1.22	−0.13	−1.66%	−0.729	0.474
$Parotid\ gland_{-R}$	26.09 ± 6.46	28.21 ± 9.87	2.12	8.13%	2.51	0.03
$Parotid\ gland_{-L}$	26.74 ± 7.10	28.63 ± 8.30	1.89	7.07%	2.19	0.04
Brainstem	28.93 ± 2.51	26.23 ± 4.55	−2.7	−9.33%	3.58	0.00
Spinal cord	19.85 ± 3.39	5.26 ± 4.74			11.99	0.0

-L, left; -R, right.

TABLE 2 Dose–volume differences of organs at risk between computed tomography and magnetic resonance imaging

Organ	DV index	CT (Gy)	MRI (Gy)	Variation (Gy)	%	*t*	*P*
$Lens_{-R}$	$Dose_{-max}$	4.08 ± 0.99	4.49 ± 1.98	0.41	10.05%	0.98	0.34
$Lens_{-L}$	$Dose_{-max}$	3.64 ± 0.66	3.82 ± 1.30	0.18	4.95%	0.74	0.47
$Optic\ nerve_{-R}$	$Dose_{-mean}$	25.03 ± 20.00	28.07 ± 20.84	3.04	12.15%	1.88	0.07
$Optic\ nerve_{-L}$	$Dose_{-mean}$	23.56 ± 20.72	28.53 ± 21.06	2.52	9.69%	1.78	0.09
$Eyeball_{-R}$	$Dose_{-mean}$	20.81 ± 9.56	20.83 ± 9.04	0.02	0.10%	−0.027	0.979
$Eyeball_{-L}$	$Dose_{-mean}$	19.80 ± 840.77	20.18 ± 0.09	0.38	1.92%	1.44	0.165
$Parotid\ gland_{-R}$	$Dose_{-mean}$	26.38 ± 2.55	31.33 ± 6.10	4.95	18.76%	3.87	0.00
$Parotid\ gland_{-L}$	$Dose_{-mean}$	26.83 ± 2.73	30.84 ± 4.92	4.01	14.95%	3.83	0.00
Brainstem	$Dose_{-0.1cm^3}$	51.05 ± 1.99	46.73 ± 11.39	−4.32	−8.46%	1.83	0.08
Spinal cord	$Dose_{-0.1cm^3}$	36.09 ± 8.11	37.68 ± 9.02	1.59	4.41%	0.53	0.60

DV, dose volume; -L, left; -R, right.

4 | DISCUSSION

With the continuous improvement of radiotherapy equipment, plan optimization, and dose calculation algorithms, precision radiation therapy for NPC has rapidly developed with more accurate and reasonable dose distribution.[23,24] In addition, the prediction model of clinical outcome and radiation injury based on modern technology will become more general and stable. At present, the accurate delineation of target volumes and OAR is the first step to evaluating radiation dose.[14,25] However, currently, it is no longer difficult to determine the target volume for NPC radiation by multimodality imaging technology, and the contouring of OAR is continuously progressing.[6,26] In addition, the advantage of MRI in contouring the OAR has been shown by different studies.[10,12,13]. In the present study, we investigated the dosimetric benefit for OAR based on MRI images.

All the patients underwent CT and MRI scanning in 1 day, and the position and range comparison results of the eyeball and lens were promising. It was shown that it is useful to consistently maintain the position of the eyeball and lens while applying the plastic film and head holder. Although, the long-term stability and reproducibility still needs to be tracked and evaluated by daily image-guided radiation therapy system.[27] The lens, eyeball, and optic nerve are easily distinguished from the background of the vitreous, aqueous humor, and orbital fat body, because they are all low-density bodies on CT; whereas vitreous and aqueous humor have low signal intensity, and orbital fat has high signal intensity on MRI T1 images. Thus, the volume difference is not significant, which is consistent with the finding of the present study, as shown in Figure 3.

The D_{mean} of the optic nerve on MRI was higher than that on CT, which can explain the extension of the optic nerve on MRI images. This is especially so in the optic nerve canal segment, which could be clearly seen, because there was no effect induced by the high-density bone tissue around the optic nerve canal.[28] Accordingly, the range of the optic nerve will be more accurate, and the extension of the optic nerve for 22 cases (right or left) demonstrates the aspect, that it is difficult to accurately outline the nerve in the optic canal by applying the simulation CT with a large bore. Indeed, it became even more important to contour the optic nerve accurately when the PTV upper boundary of the NPC was too high for the patient with a sinus invasion.

The advantages of MRI for disease detection and diagnosis of the central nervous system are well recognized. In addition, the advantage will help to determine brainstem and spinal cord imaging, as the edge of the brainstem and spinal cord could not be easily discernible on the CT because of the X-ray hardening effect caused by bone tissue.[29,30] The volume of the brainstem in the MRI images was significantly smaller than that of the CT images. It could be explained by the clear manifestation of the edge of the brainstem.

The PTV of the NPC patients was almost exactly in front of the spinal cord. Therefore, the display advantage of the spinal cord and brainstem on MRI could not produce a highly significant dosimetric benefit. The dose reduction extent of the spinal cord was less significant than the brainstem, which was associated with the relationship between the cervical spinal cord and the vertebral canal. In anatomy, the cervical cord is attached to the front edge of the vertebral canal when the patient's head and neck position are fixed by a head holder. The spinal cord is surrounded by a spinal canal bone, and the high-density bone tissue influences the display and drawing of the spinal cord. The approach that has been used for a long time to delineate the spinal cord according to the inner region of the spinal canal was not appropriate to reflect the real dose of the spinal cord because of the large spinal canal region, even though the spinal cord dose could be ensured as a safe value.[31]

There was no obvious dose deviation found with the spinal cord position offset from the second vertebral body. Thus, the neck postural stability should not be neglected. The displacement is related to the empty state of the neck from the edge of the head holder to the shoulder. There is no thermoplastic film external forces acting in the MRI scanning. Therefore, the stability of the cervical spine should be strengthened by adding an accessory device under the cervical spine for NPC patients with a head holder.

Xerostomia syndrome is the most common complication caused by radiation injury of the parotid gland during radiotherapy of NPC.[32] In the present study, the volume and mean dose of the parotid gland in MRI were greater than those in CT. The differences between CT and MRI can be explained by the recognition of the inner boundary of the parotid gland, especially for the deep lobe, which is located near the PTV.[33] For most NPC patients, the overlap of the parotid gland and the PTV is inevitable. For patients with parotid gland invasion, the part of the parotid gland with invasion should be considered as a part of the PTV, which should be given a sufficient radiation dose. Meanwhile, the most common normal parotid gland should be protected by reducing the coverage of the PTV.[34] The parotid gland should be considered as an entire volume regardless of whether it had been infiltrated or not, because the function of the partial parotid gland is unknown, so there will be more uncertainty to evaluate the incomplete gland dysfunction associated with the dose. Additionally, the radiation injury prediction model established by the dose–volume indices on the local partial volume of parotid gland was unreliable. Furthermore, the display advantage of MRI will bring promising predictive value. In the future, we will study the inner ear and temporomandibular joint, and the dose–volume variation rules applying high-resolution CT and MRI images.

In conclusion, the radiation dose evaluation of the eyeball, lens, brainstem, and spinal cord was feasible based on CT simulation images in IMRT for NPC. However, MRI images should be used to evaluate the dose for the parotid gland, brainstem, and optic nerve, particularly in patients with high radiation injury risk of these organs.

ACKNOWLEDGEMENTS

This research was supported by the National Natural Science Fund of China (No. 81301936, 81472811, and 81530060).

CONFLICT OF INTEREST

The authors declare that they had read the article and there are no competing interests.

REFERENCE

1. Chen C, Lin X, Pan J, Fei Z, Chen L, Bai P. Is it necessary to repeat CT imaging and replanning during the course of intensity-modulated radiation therapy for locoregionally advanced nasopharyngeal carcinoma? *Jpn J Radiol*. 2013;31(9):593–599.
2. Chua ML, Wee JT, Hui EP, Chan AT. Nasopharyngeal carcinoma. *The Lancet*. 2015; DOI:10.1016/S0140-6736(15)00055-0.
3. Zhou HB, Yin YF, Hu Y, et al. Suppression of vascular endothelial growth factor via siRNA interference modulates the biological behavior of human nasopharyngeal carcinoma cells. *Jpn J Radiol*. 2011;29(9):615–622.
4. Haberer-Guillerm S, Touboul E, Huguet F. Intensity modulated radiation therapy in nasopharyngeal carcinoma. *Eur Ann Otorhinolaryngol Head Neck Dis*. 2015;132(3):147–151.
5. Kong F, Ying H, Du C, et al. Patterns of local-regional failure after primary intensity modulated radiotherapy for nasopharyngeal carcinoma. *Radiat Oncol*. 2014;9:60.
6. Jager EA, Kasperts N, Caldas-Magalhaes J, et al. GTV delineation in supraglottic laryngeal carcinoma: interobserver agreement of CT versus CT-MR delineation. *Radiat Oncol*. 2015;10:26.
7. Xiao Y, Pan J, Chen Y, Lin S, et al. Prognostic value of MRI-derived masticator space involvement in IMRT-treated nasopharyngeal carcinoma patients. *Radiat Oncol*. 2015;10:204.
8. Rasch CR, Steenbakkers RJ, Fitton I, et al. Decreased 3D observer variation with matched CT-MRI, for target delineation in Nasopharynx cancer. *Radiat Oncol*. 2010;5:21.
9. Ng WT, Yuen KT, Au KH, Chan OS, Lee AW. Staging of nasopharyngeal carcinoma–the past, the present and the future. *Oral Oncol*. 2014;50(6):549–54.
10. Tao CJ, Yi JL, Chen NY, et al. Multi-subject atlas-based auto-segmentation reduces interobserver variation and improves dosimetric parameter consistency for organs at risk in nasopharyngeal carcinoma: A multi-institution clinical study. *Radiother Oncol*. 2015;115(3):407–411.
11. Sun Y, Yu XL, Luo W, et al. Recommendation for a contouring method and atlas of organs at risk in nasopharyngeal carcinoma patients receiving intensity-modulated radiotherapy. *Radiother Oncol*. 2014;110(3):390–397.
12. Liu C, Gong G, Zhou T, Wang Y, Yin Y, Li B. The error estimate for contouring the brainstem in radiotherapy of head and neck cancer: a multicenter study from north China. *J BUON*. 2014;19(2):484–489.
13. Liu C, Kong X, Gong G, Liu T, Li B, Yin Y. Error in the parotid contour delineated using computed tomography images rather than magnetic resonance images during radiotherapy planning for nasopharyngeal carcinoma. *Jpn J Radiol*. 2014;32(4):211–216.
14. Jeraj R, Cao Y, Ten Haken RK, Hahn C, Marks L. Imaging for assessment of radiation-induced normal tissue effects. *Int J Radiat Oncol Biol Phys*. 2010;76(3 Suppl):S140–S144.
15. Deasy JO, Bentzen SM, Jackson A, et al. Improving normal tissue complication probability models: the need to adopt a "data-pooling" culture. *Int J Radiat Oncol Biol Phys*. 2010;76(3 Suppl):S151–S154.
16. Merlotti A, Alterio D, Vigna-Taglianti R, et al. Technical guidelines for head and neck cancer IMRT on behalf of the Italian association of radiation oncology - head and neck working group. *Radiat Oncol*. 2014;9:264.
17. Bortfeld T, Schmidt-Ullrich R, De Neve W. *Image-Guided IMRT*. Germany:Springer Berlin Heidelberg 2006.
18. Lu H, Lin H, Feng G, et al. Interfractional and intrafractional errors assessed by daily cone-beam computed tomography in nasopharyngeal carcinoma treated with intensity-modulated radiation therapy: a prospective study. *J Radiat Res*. 2012;53(6):954–960.
19. Tang JM, Ma XM, Hou YL, et al. Analysis of simultaneous modulated accelerated radiotherapy (SMART) for nasopharyngeal carcinomas. *J Radiat Res*. 2014;55(4):794–802.
20. Kirkpatrick, JP, van der Kogel, AJ, Schultheiss, TE. Radiation dose-volume effects in the spinal cord. *Int J Radiat Oncol Biol Phys*. 2010;76(3 Suppl):S42–S49.
21. Deasy JO, Moiseenko V, Marks L, Chao KS, Nam J, Eisbruch A. Radiotherapy dose-volume effects on salivary gland function. *Int J Radiat Oncol Biol Phys*. 2010;76(3 Suppl):S58–S63.
22. Mayo, C, Yorke, E, Merchant, TE. Radiation associated brainstem injury. *Int J Radiat Oncol Biol Phys*. 2010;76(3 Suppl):S36–S41.
23. Chitapanarux I, Chomprasert K, Nobnaop W, et al. A dosimetric comparison of two-phase adaptive intensity-modulated radiotherapy for locally advanced nasopharyngeal cancer. *J Radiat Res*. 2015;56(3):529–538.
24. White P, Chan KC, Cheng KW, Chan KY, Chau MC. Volumetric intensity-modulated arc therapy vs conventional intensity-modulated radiation therapy in nasopharyngeal carcinoma: a dosimetric study. *J Radiat Res*. 2013;54(3):532–545.
25. Wang W, Yang H, Mi Y, et al. Rules of parotid gland dose variations and shift during intensity modulated radiation therapy for nasopharyngeal carcinoma. *Radiat Oncol*. 2015;10:3.
26. Yang Z, Shi Q, Zhang Y, et al. Pretreatment (18)F-FDG uptake heterogeneity can predict survival in patients with locally advanced nasopharyngeal carcinoma–a retrospective study. *Radiat Oncol*. 2015;10:4.
27. Via R, Fassi A, Fattori G, et al. Optical eye tracking system for real-time noninvasive tumor localization in external beam radiotherapy. *Medical physics*. 2015;42(5):2194–2202.
28. Toosy, AT, Mason, DF, Miller, DH. Optic neuritis. *Lancet Neurol*. 2014;13(1):83–99.
29. Shenton ME, Hamoda HM, Schneiderman JS, et al. A review of magnetic resonance imaging and diffusion tensor imaging findings in mild traumatic brain injury. *Brain Imaging Behav*. 2012;6(2):137–192.
30. Stroman PW, Wheeler-Kingshott C, Bacon M, et al. The current state-of-the-art of spinal cord imaging: methods. *NeuroImage*. 2014;84:1070–1081.
31. Kong FM, Ritter T, Quint DJ, et al. Consideration of dose limits for organs at risk of thoracic radiotherapy: atlas for lung, proximal bronchial tree, esophagus, spinal cord, ribs, and brachial plexus. *Int J Radiat Oncol Biol Phys*. 2011;81(5):1442–1457.
32. Pow EH, Kwong DL, McMillan AS, et al. Xerostomia and quality of life after intensity-modulated radiotherapy vs. conventional radiotherapy for early-stage nasopharyngeal carcinoma: initial report on a randomized controlled clinical trial. *Int J Radiat Oncol Biol Phys*. 2006;66(4):981–991.
33. Bag AK, Cure JK, Chapman PR, Pettibon KD, Gaddamanugu S. Practical imaging of the parotid gland. *Curr Probl Diagn Radiol*. 2015;44(2):167–192.
34. Cao CN, Luo JW, Gao L, et al. Clinical characteristics and patterns of failure in the parotid region after intensity-modulated radiotherapy for nasopharyngeal carcinoma. *Oral Oncol*. 2013;49(6):611–614.

How to cite this article: Gong G, Kong X, Wang X, Zheng C, Guo Y, Yin Y. Finding of dose evaluation for organs at risk in intensity-modulated radiation therapy for nasopharyngeal carcinoma using magnetic resonance imaging. *Prec Radiat Oncol*. 2017;1:7–12. https://doi.org/10.1002/pro6.6